THE JOURNAL OF BIOLOGICAL CHEMISTRY VOL. 290, NO. 17, pp. 10876–10890, April 24, 2015

Multidomain Human Peroxidasin 1 Is a Highly Glycosylated and Stable Homotrimeric High Spin Ferric Peroxidase*

Received for publication, December 15, 2014, and in revised form, February 18, 2015 Published, JBC Papers in Press, February 24, 2015, DOI 10.1074/jbc.M114.632273

Monika Soudi[‡], Martina Paumann-Page[‡], Cedric Delporte[§1], Katharina F. Pirker[‡], Marzia Bellei[¶], Eva Edenhofer[‡], Gerhard Stadlmayr[‡], Gianantonio Battistuzzi[‖], Karim Zouaoui Boudjeltia[**], Paul G. Furtmüller[‡], Pierre Van Antwerpen[§], and Christian Obinger[‡2]

From the [‡]Department of Chemistry, Division of Biochemistry, BOKU-University of Natural Resources and Life Sciences, Muthgasse 18, A-1190 Vienna, Austria, the [§]Laboratory of Pharmaceutical Chemistry and Analytical Platform of the Faculty of Pharmacy, Faculty of Pharmacy, Université Libre de Bruxelles, 1050 Brussels, Belgium, the Departments of [¶]Life Sciences and [‖]Chemistry and Geology, University of Modena and Reggio Emilia, 41125 Modena, Italy, and the [**]Laboratory of Experimental Medicine (ULB 222 Unit), CHU de Charleroi, A. Vésale Hospital, Université Libre de Bruxelles, 6110 Montigny-le-Tilleul, Belgium

Background: Human peroxidasin 1 (hsPxd01) mediates the formation of sulfilimine cross-links within the collagen IV scaffold of basement membranes.
Results: Overexpressed hsPxd01 contains covalently linked heme catalytically active for production of hypobromous acid.
Conclusion: hsPxd01 has peroxidase-like active site structure but restricted substrate accessibility.
Significance: Architecture of hsPxd01 facilitates product release and its interactions with the physiological substrate collagen IV.

Human peroxidasin 1 (hsPxd01) is a multidomain heme peroxidase that uses bromide as a cofactor for the formation of sulfilimine cross-links. The latter confers critical structural reinforcement to collagen IV scaffolds. Here, hsPxd01 and various truncated variants lacking nonenzymatic domains were recombinantly expressed in HEK cell lines. The *N*-glycosylation site occupancy and disulfide pattern, the oligomeric structure, and unfolding pathway are reported. The homotrimeric iron protein contains a covalently bound ferric high spin heme per subunit with a standard reduction potential of the Fe(III)/Fe(II) couple of −233 ± 5 mV at pH 7.0. Despite sequence homology at the active site and biophysical properties similar to human peroxidases, the catalytic efficiency of bromide oxidation (k_{cat}/K_M^{app}) of full-length hsPxd01 is rather low but increased upon truncation. This is discussed with respect to its structure and proposed biosynthetic function in collagen IV cross-linking.

Heme peroxidases are versatile enzymes abundant in all kingdoms of life necessary for manifold physiological functions. Several superfamilies and families have been described that evolved independently during evolution. Chordata peroxidases like myeloperoxidase (MPO),[3] eosinophil peroxidase (EPO), lactoperoxidase (LPO), and thyroid peroxidase (TPO) have been shown to play important roles in innate immunity as well as hormone biosynthesis (1, 2). Recently, a phylogenetic study demonstrated that these vertebrate enzymes are part of a superfamily that is composed of seven subfamilies (3). In a close phylogenetic neighborhood of the above-mentioned chordata peroxidases (*i.e.* subfamily 1), multidomain peroxidases called peroxidasins are clustering in subfamily 2. This name was first coined in 1994 by Nelson *et al.* (4), who succeeded in identifying the first representative in *Drosophila melanogaster*. They described this peroxidasin as a multidomain peroxidase that participates in extracellular matrix consolidation. In the following 15 years, only a few papers were published reporting the occurrence of peroxidasins in other organisms like *Caenorhabditis elegans* (5) or *Xenopus tropicalis* (6) and suggesting a role in extracellular matrix biosynthesis. Finally, in 2008, the two human peroxidasins (hsPxd01 and hsPxd02) became the focus of investigations analyzing expression patterns (7–10) and biochemical properties (7, 8, 11, 12).

Great attention was devoted to human peroxidasin 1 after publication of the work by Bhave *et al.* (13) that demonstrated the responsibility of hsPxd01 for the formation of sulfilimine bonds in collagen IV via release of hypohalous acids. Furthermore, it was shown that this unique covalent bond in basement membrane is a primordial innovation for tissue evolution (14). Moreover, very recently it could be demonstrated that bromide oxidation to hypobromous acid mediated by hsPxd01 is essential for the assembly of collagen IV scaffolds in tissue development and architecture (15).

Fig. 1 depicts the multidomain structure of human peroxidasin 1. Gene analysis shows the occurrence of a signal peptide, one leucine-rich repeat domain (LRR), four immunoglobulin-like motifs (Ig), a peroxidase domain (POX), and a C-terminal von Willebrand factor C domain (VWC). Despite the important physiological implications, no detailed structural information

* This work was supported in part by Austrian Science Fund Project P25538, Doctoral Program BioToP-Biomolecular Technology of Proteins Grant FWF W1224, Belgian Fund for Scientific Research Grant 34553.08, and a grant from the Fond d'Encouragement à la Recherche 2007 (Université Libre de Bruxelles).
[1] Postdoctoral researcher funded by the Belgian Fund for Scientific Research.
[2] To whom correspondence should be addressed. Tel.: 43-1-47654-6073; Fax: 43-1-47654-6059; E-mail: christian.obinger@boku.ac.at.
[3] The abbreviations used are: MPO, myeloperoxidase; hsPxd01, human peroxidasin 1; hsPxd01-con 4, construct 4 of human peroxidasin 1; POX, peroxidase domain; LRR, leucine-rich repeat; VWC, von Willebrand factor C; LPO, lactoperoxidase; EPO, eosinophil peroxidase; ECD, electronic circular dichroism; SEC, size exclusion chromatography; MALS, multiangle light scattering; DSC, differential scanning calorimetry; PDB, Protein Data Bank; PNGase F, peptide:*N*-glycosidase F.

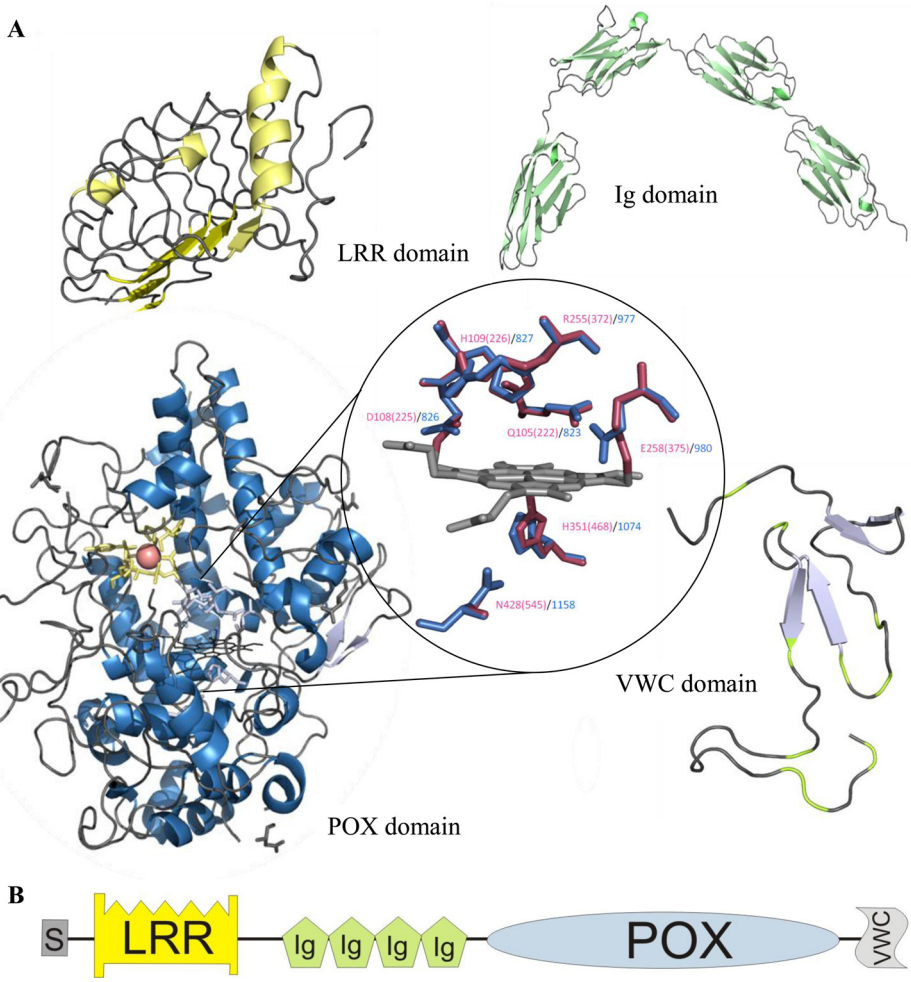

FIGURE 1. **Arrangement and composition of domains of hsPxd01.** *A,* models are of the following: (i) LRR domain, including N- and C-terminal capping motifs; (ii) four consecutive Ig domains; (iii) VWC domain with highlighted cysteines; and (iv) of the peroxidase domain. The latter model was constructed using homologous goat LPO (PDB code 2R5L) as template. Magnified overlay of the active site of goat LPO(*gLPO*) and hsPxd01 illustrates the conservation of all amino acids in the active site. Numbers in *blue* correspond to hsPxd01 amino acid sequence, including the signal peptide, and numbers in *pink* correspond to gLPO amino acid sequence with (in *parentheses*) and without signal and propeptide region. *B,* domain arrangement of human peroxidasin 1.

about human peroxidasin 1 is available. This prompted us to study the biophysical and biochemical characteristics of human peroxidasin 1 for a better understanding of its mode of function and mechanism.

EXPERIMENTAL PROCEDURES

Materials and Reagents—Ammonium bicarbonate, formic acid, methanol, and acetonitrile were from Merck. 2,2,2-Trifluoroethanol, iodoacetamide, trypsin (from bovine pancreas and treated with L-1-tosylamide-2-phenylethyl chloromethyl ketone), pepsin, and PNGase F (from *Elizabethkingia meningoseptica*) were from Sigma. Water was purified using a Milli-Q purification system (Millipore, Bedford, MA).

Three-dimensional Structural Models of hsPxd01 Domains—Models of distinct human peroxidasin 1 domains were generated using the ESyPred3D server (16). Amino acid identities of the hsPxd01 domains with the respective templates of LRR (PDB code 2O6S), Ig (PDB code 3B43), POX (PDB code 2R5L), and VWC (PDB code 1U5M) domains were 31.8, 21.1, 39.7, and 30.7%, respectively.

Cloning, Stable Transfection, Expression, and Purification of hsPxd01—Full-length human peroxidasin 1 encoded on a pcDNA^{TM}3.1/V5-His TOPO vector was kindly provided by Miklós Geiszt (Department of Physiology, Semmelweis University School of Medicine, Budapest, Hungary). For the stable calcium phosphate transfection of HEK 293 cells, standard selection and cultivation procedures with minor modifications were used (17). After screening of the stably transfected clones by immunoblotting as well as peroxidase activity screening, the best producer was selected for large scale production in triple flasks (Life Technologies). During production, cells were cultivated in DMEM supplemented with 10% fetal bovine serum, 5 μg/ml hematin, penicillin, and streptomycin and a protease inhibitor mixture (Sigma). The harvested media were stored at 4 °C and eventually purified using immobilized metal affinity chromatography. Therefore, the harvested media were supplemented with 300 mM NaCl, 40 mM imidazole, and pH adjusted to 7.4 before application onto a chelating Sepharose gel column (GE Healthcare). The column was charged with Ni^{2+} and equilibrated with 20 mM phosphate buffer, pH 7.4, with 300 mM NaCl and 40 mM imidazole. Protein was

eluted with 20 mM phosphate buffer containing 500 mM NaCl and 300 mM imidazole. Fractions with the best purity number were pooled, concentrated, and desalted using Centricon with a 100-kDa cutoff membrane (Millipore).

Cloning, Transient Transfection, and Expression of hsPxd01 and Truncated Constructs—DNA of hsPxd01 and its truncated versions were cloned into a modified pTT5 vector (NRC-BRI) containing a C-terminal Strep tag to facilitate purification. Six different constructs were designed and cloned, including the complete protein hsPxd01-con1 (LRR-Ig-POX-VWC, 1453 amino acids), hsPxd01-con2 omitting the LRR domain (Ig-POX-VWC, 1234 amino acids), hsPxd01-con3 excluding the C-terminal VWC domain (LRR-Ig-POX, 1288 amino acids), and hsPxd01-con4 omits both domains (Ig-POX, 1069 amino acids). hsPxd01-con5 (695 amino acids) and hsPxd01-con6 (593 amino acids) consist only of the peroxidase domain, including or excluding the homologous propeptide region, respectively. The forward and reverse primers used for the construct preparations were as follows: 5′-ATGCGCTAGCGTGGTGGCCCAGAAGCCGGGCGCAGGGTGTCCG-3′ and 5′-ATGCGGTACCGGGCTTTTCCTCCGCCCTCTTCTGTAAGCAGACTGG-3′ for hsPxd01-con1; 5′-ATGCGCTAGCCCCCGGATCACCTCCGAGCCCCAGGACGCAGATGTGACC-3′ and 5′-ATGCGGTACCGGGCTTTTCCTCCGCCCTCTTCTGTAAGCAGACTGG-3′ for hsPxd01-con2; 5′-ATGCGCTAGCGTGGTGGCCCAGAAGCCGGGCGCAGGGTGTCCG-3′ and 5′-ATGCGGTACCGTCCTGCCACACCCGGAGGTCCACCCTGGGG-3′; 5′-ATGCGCTAGCCCCCGGATCACCTCCGAGCCCCAGGACGCAGATGTGACC-3′ and 5′-ATGCGGTACCGTCCTGCGGG-3′; 5′-ATGCGCTAGCGGAGATCCGTTTGTAGCTACCTCCATCGTGG-3′ and 5′-ATGCGGTACCGTCCTGCCACACCCGGAGGTCCACCCTGGGG-3′; and 5′-ATGCGCTAGCGGCTGTACCGCCCACCGGCGCGTGAACAACTGC-3′ and 5′-ATGCGGTACCGTCCTGCCACACCCGGAGGTCCACCCTGGGG-3′ for constructs 3–6, respectively. For the determination of the thermal stability and bromination activity as described below, a hsPxd01-con4 version with N-terminal polyhistidine tag for easy purification and HRV-3C cleavage site for tag removal was used. The following two primers were employed for PCR amplification: 5′-ATGCGCTAGCCATCATCACCATCACCATCACCATCTGGAAGTACTTTTTCAGGGGCCCCCCCGGATCACCTCCGAGCCCCAGGACGCAGATGTGACC-3′ and 5′-ATGCGCGGCCGCTTATCAATGGTGATGGTGATGATGGTCCTGCCACACCCGGAGGTCCACCCTGGGG-3′. The measurements were conducted without prior polyhistidine tag removal. The plasmid preparation as well as PCR and restriction screening were carried out in *Escherichia coli* TOP10 cells. Before endotoxin-free maxi preparation of plasmid DNA (Qiagen, Macherey-Nagel) for transient transfection, the respective constructs were validated by DNA sequencing. HEK 293 6E cells (NRC-BRI) were cultivated as described previously (18, 19) using F17 media (Life Sciences) with 0.1% pluronic F68 agent (Gibco), 4 mM L-glutamine (Gibco) and 50 μg/ml geneticin. For transfection, standard procedures for the recombinant production of secreted proteins were followed with minor variations. For varying cell culture volumes, the procedures were scaled up or down accordingly. To improve heme incorporation into the peroxidase domain, 5 μg/ml hematin was added 4 h post-transfection. Cell supernatant was harvested 5 days post-transfection.

SDS-PAGE, Western Blot, and Multiangle Light Scattering—Protein samples were separated by gradient PAGE and analyzed either directly using Coomassie Blue staining or after immunoblotting onto a nitrocellulose membrane (GE Healthcare) using anti-His (Qiagen), anti-Strep (IBA), or anti-hsPxd01 antibodies (Sigma). Standard protocols were followed.

For determination of the molar mass, the protein samples were analyzed by SEC chromatography coupled to detectors for analysis of UV-visible, refraction index, and multiangle light scattering (MALS). For instrumentation, HPLC (Shimadzu prominence LC20) and MALS (WYATT Helios Dawn8+ plus QELS; software ASTRA 6) were used, and the columns were WYATT SEC Columns (7.8 × 5 and 7.8 mm × 300 mm; particle size, 5 μm, pore size 300 Å) with corresponding guard column (WTC030S5G). SEC buffer was Dulbecco's PBS plus 200 mM NaCl; flow rate was 0.5 ml per min; injected protein was 55 μg. For performance of SEC chromatography under reducing conditions, the protein was pretreated with 50 mM dithiothreitol (DTT) for 30 min at room temperature, and during chromatography, the SEC buffer contained 2 mM DTT.

Assessment of Heme to Protein Linkage by Enhanced Chemiluminescence (ECL)—MPO and hsPxd01 samples were heated for 10 min at 70 °C before separation by gradient PAGE. Then the gel was blotted on nitrocellulose membrane, and the covalent heme to protein was probed by ECL detection (20). Clarity Western ECL (Bio-Rad) substrate was used as recommended, and signals were detected with a ChemiDoc XRS+ imaging system (Bio-Rad).

Mass Spectrometric Analysis of Glycosylation Occupancy—After precipitation by 10% trichloroacetic acid, recombinant hsPxd01 pellets were dissolved in the denaturation buffer ammonium bicarbonate (100 mM) and 2,2,2-trifluoroethanol and subsequently reduced by DTT. Alkylation was performed with iodoacetamide, and the excess was quenched again by DTT. Before addition of trypsin or pepsin, the sample was diluted 10 times, and the pH was adjusted to the corresponding optimum. After overnight incubation at 37 °C, the proteases were heat-inactivated. Finally, PNGase F was added and incubated overnight at 37 °C.

For *N*-glycan site occupancy, a rapid resolution liquid chromatographic system (1200 series) coupled to a quadrupole/time-of-flight equipped with an electrospray ionization source (ESI-QTOF 6520 series) mass spectrometer (Agilent Technologies, Palo Alto, CA) was used for analysis of the aforementioned protein digests (21). As PNGase F removes glycans and performs deamination of asparagine (Asn → Asp), the glycosylation occupancy was calculated by measuring the ratio between the area under the curve of the native peptide and its deaminated form. Total occupancy (100%) was obtained when the deaminated form of the peptide alone was detected. A glycosylation site free of glycans (0% of occupancy) was obtained when only the peptide with the native Asn residue was present. For prediction of glycosylation sites NetNgly was used (22).

Mass Spectrometric Analysis of Cysteines and Cystines—Analysis of cysteine residues was carried out on hsPxd01 according to a method previously described for sequence recovery (23). The method was adjusted to allow for the recovery of free cysteines as carbamidomethylated cysteines, whereas disulfide bonds were conserved. Briefly, recombinant hsPxd01 (350 μg) was incubated at 20 °C in darkness for 10 h in 25 μl of 100 mM ammonium bicarbonate, including 60 mM iodoacetamide. 25 μl of 2,2,2-trifluoroethanol, 300 μl of formic acid (2% (v/v) in water), and 300 μl of pepsin (5 mg/ml in formic acid 2% (v/v) in water) were added, and hsPxd01 was digested overnight at 37 °C. After pepsin heat inactivation, pH was adjusted to 7–8, and PNGase F (100 milliunits) was added to proceed to peptide deglycosylation for 7 h at 37 °C. Finally, trypsin (50 μl, 1 mg/ml) was added, and overnight digestion was performed at 37 °C. Trypsin was inactivated by addition of 2 μl of formic acid (100% (v/v)), and sample was dried down using a centrifuge vacuum. Sample was finally dissolved in 200 μl of formic acid (0.1% (v/v) in water). Free cysteines are detected in an alkylated form (carbamidocysteine).

30 μl of the resulting samples were injected into the LC system and analyzed as described previously (23). Briefly, analyses were performed with the rapid resolution liquid chromatographic ESI-QTOF system described above. Peptides were separated on a Poroshell-120 end-capped C18 (100 × 2.1 mm inner diameter, 2.7-μm particle size) from Agilent Technologies (Palo Alto, CA) using a 105-min gradient of formic acid and acetonitrile (23). Auto-MS/MS spectra were acquired in positive and high resolution acquisition mode (4 GHz) (23). Data were acquired by the Mass Hunter Acquisition® for TOF and QTOF (version B.04 SP3) software and analyzed by the Mass Hunter Qualitative Analysis (version B.05 SP1) with Bioconfirm® and by Spectrum Mill® software (Agilent Technologies, Palo Alto, CA).

Electron Paramagnetic Resonance Spectroscopy (EPR)—Purified recombinant hsPxd01 and hsPxd01-con4 were prepared in 40 mM citrate/phosphate buffer, pH 7, and 20% glycerol (Sigma) as cryoprotectant. The sample was transferred into Wilmad quartz tubes (3 mm inner diameter) and flash-frozen in liquid N_2. Frozen samples were kept frozen on dry ice while the headspace above the sample was flushed with argon. Oxygen-free samples were frozen back to 77 K and transferred into the resonator for 10 K measurements. Spectra were recorded on a Bruker EMX continuous wave EPR spectrometer, operating at X-band (9 GHz) frequencies, equipped with a high sensitivity resonator and an Oxford Instruments ESR900 cryostat. EPR spectra were recorded under nonsaturating conditions using 2 milliwatts microwave power, 100 kHz modulation frequency, 1 millitesla modulation amplitude, 41-ms conversion time, 41-ms time constant, and 2048 points. Simulation of high spin Fe(III) forms was carried out using the software EasySpin (24) and consisted of a weighted sum of simulations of the individual high spin compounds. The rhombicity was obtained from g_x^{eff} and g_y^{eff} (25), and the relative intensities were calculated on the basis of the simulations.

Spectroelectrochemistry—The standard reduction potential, E'_0, determination was performed using a homemade optically transparent thin layer spectroelectrochemical cell (26–28). Spectroelectrochemical titrations were carried out at 25 °C using 1-ml samples containing 5 μM hsPxd01 or hsPxd01-con4 dissolved in 100 mM phosphate buffer and 100 mM NaCl, pH 7.4, in the presence of 30 μM methyl viologen and 1 μM lumiflavine 3-acetate, methylene blue, phenazine methosulfate, and indigo disulfonate as mediators.

Determination of Thermal Stability—Temperature-mediated protein unfolding was followed either by electronic circular dichroism (ECD) spectroscopy or differential scanning calorimetry (DSC). For ECD, Chirascan from Applied Photophysics (Leatherhead, UK) was used, and changes of the ellipticity at 208 nm as well as at 412 nm in 20 mM phosphate buffer, pH 7.4, with increasing temperature were recorded and evaluated (29). The instrument was flushed with nitrogen at a flow rate of 5 liters min^{-1} and was equipped with a Peltier element for temperature control. Temperature-mediated denaturation was monitored between 20 and 95 °C. Temperature was increased stepwise with 1.0 °C min^{-1}. Single wavelength scans were performed with instrumental parameters set as follows. Visible ECD at Soret maximum was performed with 9.5 μM hsPxd01 in 20 mM phosphate buffer, pH 7.4. The path length was 10 mm and spectral bandwidth 1 nm, and scan time per point was set at 10 s. Far-UV ECD at 208 nm was performed with 4.8 μM hsPxd01 in 20 mM phosphate buffer, pH 7.4. The path length was 1 mm and spectral bandwidth 3 nm, and scan time per point was set at 10 s.

DSC analysis was done with a VP-DSC Capillary Cell Microcalorimeter (MicroCal). 5 μM protein samples in 20 mM phosphate buffer, pH 7.4, were heated from 30 to 100 °C with a heating rate of 1 °C min^{-1}. Baselines were subtracted and data normalized for protein concentration and fitted with a non-two-state thermal unfolding model using the software Origin 7.

Determination of Bromination Activity—Bromination activity of recombinant hsPxd01 and hsPxd01-con4 was tested spectrophotometrically by measuring the halogenation of NADH. The produced hypobromous acid reacts with NADH to stable bromohydrin. This assay detects the initial rate of bromohydrin production at $\lambda = 275$ nm using ϵ_{275} of 11,800 M^{-1} cm^{-1} (30–32). Bromide was chosen because it was shown to be an essential trace element for assembly of collagen IV scaffolds in tissue development and architecture (15). Briefly, 100 nM hsPxd01 or hsPxd01-con4 was incubated at 25 °C in 20 mM phosphate buffer, pH 7.4, containing 100 μM NADH and varying concentrations of either hydrogen peroxide (with a constant NaBr concentration of 5 mM) or NaBr (with a constant hydrogen peroxide concentration of 50 μM) (32). Reactions were started upon addition of H_2O_2. Initial rates were measured over the 1st min of reaction to minimize possible inhibition by hydrogen peroxide. Note that Michaelis-Menten parameters (K_m and V_{max}) derived from steady-state rate measurements do not conform to reactions catalyzed by peroxidases, which follow an irreversible ping-pong mechanism (where equilibria between reactants and products are not established). Nevertheless, to allow the comparison of the bromination activity of hsPxd01 with data from peroxidases investigated under the same assay conditions (32) and to keep the kinetic model as simple as possible, we present K_M^{app} and V_{max}^{app} values, which were determined using nonlinear regression (Sigma Plot, Jandel Scientific). Here, the

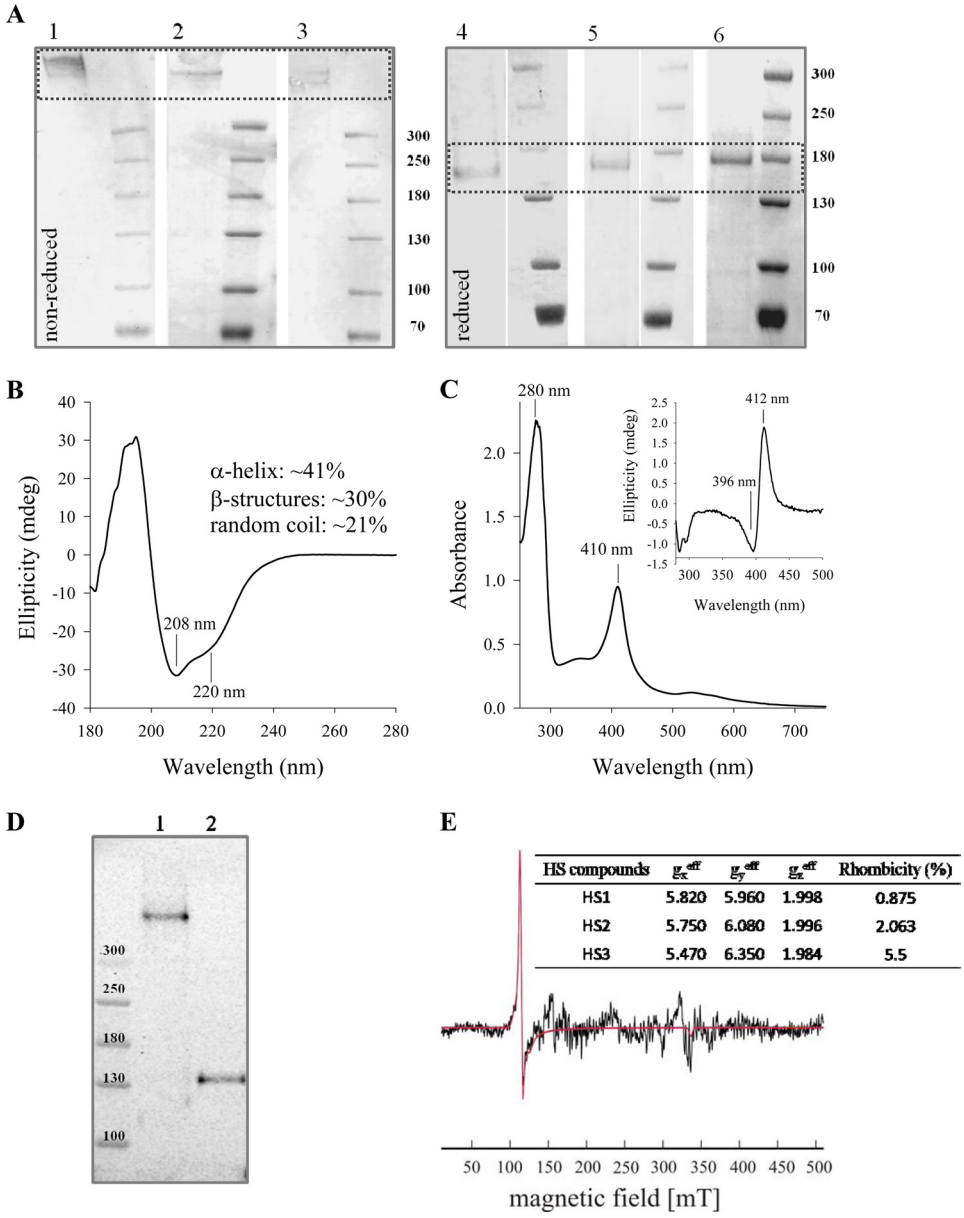

FIGURE 2. **Structural and spectral properties of human peroxidasin 1.** *A,* SDS-PAGE (3–8% gradient polyacrylamide) of hsPxd01 purified from stably transfected HEK 293 cells under nonreducing (*left panel*) and reducing conditions (*right panel*). The gel was stained with anti-Pxd antibody (*lanes 1* and *4*), anti-His antibody (*lanes 2* and *5*), and Coomassie Blue (*lanes 3* and *6*). *B,* far-UV CD spectrum of 4.8 μM recombinant hsPxd01 (20 mM phosphate buffer, pH 7.4). Additionally, the calculated overall secondary structure composition is depicted. *C,* UV-visible spectrum of 9.5 μM recombinant hsPxd01 in 20 mM phosphate buffer, pH 7.4. The *inset* shows the corresponding CD spectrum in the visible region. *D,* covalent heme to protein linkage detected by enhanced chemiluminescence under nonreducing conditions with heated samples of full-length hsPxd01 (*lane 1*) and hMPO (*lane 2*). *E,* representative experimental EPR spectrum (*black line*) of 20 μM hsPxd01 at 10 K (40 mM citrate/phosphate buffer, pH 7, 20% glycerol) using 30 scans. The simulated spectrum (*red line*) as sum of three individual high spin species clearly indicates ligand coordination of axial symmetry. The simulation parameters of these high spin forms used for simulation as well as the minor contribution (%) from rhombic ligand coordination are also shown.

K_M^{app} value simply represents the substrate concentration where the overall rate is half of its maximum value, and the V_{max}^{app} value represents the limiting step of the overall reaction at certain enzyme and substrate concentrations. Importantly, no reaction was observed upon mixing of only NADH, hydrogen peroxide, and hsPxd01 or hsPxd01-con4.

RESULTS

Properties of Recombinant Protein and Oligomeric Structure—The average yield of recombinant hsPxd01 produced in HEK 293 cells by stable transfection was 0.5–0.9 mg per liter of harvested media. Recombinant human peroxidasin 1 (hsPxd01) either produced by stable or transient transfection applied to SDS-PAGE had a molar mass of >500 kDa (Fig. 2*A*, *lanes 1–3*). The theoretical molar mass of the protein (1445 amino acids without signal peptide, see also Fig. 5) is 163 kDa. Under reducing conditions, the protein band is found at ~180 kDa (Fig. 2*A*, *lanes 4–6*), suggesting that hsPxd01 is an oligomeric protein with monomers being linked by DTT-sensitive covalent bonds. The gels were stained with anti-hsPxd01 antibody (Fig. 2*A*, *lanes 1* and *4*), anti-His antibody (*lanes 2* and *5*), and Coomassie Blue (*lanes 3* and *6*).

The far-UV ECD spectrum of recombinant hsPxd01 showed a clear minimum at 208 nm as well as a shoulder at 220 nm and a maximum around 195 nm corresponding to an overall secondary structure composition of 41% α-helices and 30% β-sheets (Fig. 2*B*). Purified recombinant hsPxd01 had a Soret band at 410 nm and additional bands at 529, 563, and 627 nm. Very similar spectra were obtained for the construct hsPxd01-con4 (data not shown). The average Reinheitszahl (purity number, *i.e.* $A_{410\,nm}/A_{280\,nm}$) of hsPxd01 varied between 0.41 and 0.47 corresponding to 72–81% heme occupancy. Molar extinction coefficients at 280 and 410 nm using the Bradford protein assay were determined to be 163,000 and 89,000 M^{-1} cm^{-1}, respectively. The spectrum of a representative preparation is depicted in Fig. 2*C*. The ECD spectrum in the visible region shows a minimum at 396 nm and a maximum at 412 nm (*inset* to Fig. 2*C*). The heme in hsPxd01 (as well as in the constructs) is covalently linked as demonstrated in Fig. 2*D*. Continuous wave low temperature EPR spectra of hsPxd01 at pH 7 demonstrates the presence of mostly high spin Fe(III). Fig. 2*E* depicts a representative experimental spectrum of 20 μM hsPxd01 as well as the simulated spectrum (*red line*) as sum of individual high spin species clearly indicating ligand coordination of axial symmetry. A similar high spin Fe(III) spectrum was also obtained with hsPxd01-con4 (data not shown). Depending on the protein batch, a minor contribution of low spin species was observed in both proteins.

To obtain the exact molar mass and oligomeric composition, purified recombinant hsPxd01 was analyzed by HPLC combined with UV-visible, refraction index, and MALS detectors. Fig. 3*A* shows that the protein eluted as a single peak at a retention time of 14.35 min. With SEC-MALS, an average size of 504 kDa was obtained, which is in accordance with a homotrimeric structure (Fig. 3*B*). When SEC was performed under reducing conditions, the most prominent peak eluted at 18.54 min with an average size of 175 kDa. These data clearly demonstrate that this human multidomain peroxidase is a homotrimeric and glycosylated protein. Glycosylation contributes with about 12 kDa to the total molar mass of hsPxd01.

Next, we were interested in which domains were involved in the covalent linkage between the three monomers. Different (truncated) constructs were designed (summarized in Fig. 4*A*) and transiently expressed in HEK 293 6E cells. Briefly, besides the complete protein (hsPxd01) variants without the VWC domain (hsPxd01-con3), without LRR and VWC domains (hsPxd01-con4), without LRR, Ig, and VWC domains (hsPxd01-con5), and without LRR, Ig and VWC domains and the propeptide N-terminal of the peroxidase domain (hsPxd01-con6) were produced (Fig. 4*B*). The media of small scale experiments were harvested and directly applied to SDS-PAGE without any further purification step. Under nonreducing conditions the presence of trimeric hsPxd01 was visible, whereas hsPxd01-con3, hsPxd01-con4, and hsPxd01-con5 are monomeric (compare *upper panels* (Coomassie Blue staining) with *lower panels* (immunoblotting) in Fig. 4*B*). Under reducing conditions a similar pattern was obtained except for the full-length protein, which now gave a band at 180 kDa. In the case of hsPxd01-con6, various bands at a higher molar mass range appeared indicating instability and aggregation. Because the yield of this construct was poor compared with the other constructs, this might indicate that the homologous propeptide region contributed to the conformational stability. However, the main conclusion from these data is that in the absence of the VWC domain the constructs were monomeric, clearly suggesting that hsPxd01 is a homotrimeric protein having the monomers covalently linked by disulfide bridges between their C-terminal VWC domains.

N-Glycosylation Site Occupancy and Disulfide Pattern of Human Peroxidasin 1—Computationally, 11 *N*-glycosylation sites were predicted for hsPxd01 (Fig. 5). The first one (Asn-390) was located at the second Ig domain on the loop between the C- and D-strand (similar to CH2 glycosylation in IgG1-Fc). In the peroxidase domain seven N*X*(S/T) motifs were found, four in propeptide region (Asn-640, Asn-699, Asn-719, and Asn-731) and four in the core of the peroxidase domain (Asn-865, Asn-964, Asn-1178, and Asn-1280). Two further *N*-glycosylation sites were predicted to be at the linker between the peroxidase domain and the VWC domain (Asn-1368) as well as on the VWC module itself (Asn-1425) (Fig. 5).

For experimental verification, hsPxd01 was proteolytically cleaved by either pepsin or trypsin, deglycosylated using PNGase F, and analyzed by mass spectrometry. Table 1 presents a detailed list of identified peptides and their glycosylation status. Glycosylation occupancy was assessed by deamination of asparagines (Asn→Asp) due to glycan removal by PNGase F.

Data demonstrate that except for Asn-964, all other sites were *N*-glycosylated, four completely (Asn-640, Asn-731, Asn-865, and Asn-1425), whereas the others were found partially glycosylated. Table 1 depicts the relative occupancy in both digests. For example, more than 70% of the recovered peptides at Asn-390, Asn-699, Asn-1178, and Asn-1280 were glycosylated, whereas Asn-719 was mostly nonglycosylated (peptic digest, 100%; tryptic digest, 86.59%).

Furthermore, we analyzed which cysteines are involved in disulfide bridges. Mass spectrometric analysis of recombinant hsPxd01 demonstrated that Cys-12 and Cys-20 (signal peptide), Cys-736 and Cys-970 (peroxidase domain), and Cys-1315, Cys-1316, and Cys-1319 (VWC domain) are free cysteines as demonstrated by the presence of alkylation (Table 2). This suggests that the other cysteines are involved in disulfide bond formation as has been proposed by Uniprot (33). From the 20 predicted bound cysteines, 12 could be confirmed by MS. Confirmed disulfide bridges include Cys-36–Cys-42, Cys-40–Cys-49, Cys-196–Cys-243, and Cys-198–Cys-222 (LRR domains), Cys-267–Cys-317 and Cys-454–Cys-502 (IgG domains), Cys-620–Cys-721 (propeptide region of peroxidase domain), and Cys-723–Cys-885, Cys-732–Cys-748, Cys-847–Cys-857, Cys-851–Cys-875, Cys-1177–Cys-1234, and Cys-1275–Cys-1301 (peroxidase domain) (Table 2). Eight predicted disulfide bridges could not be found, two in the IgG-like domains, one in the peroxidase domain, and five in the VWC domain. This does not mean that they are not present because during sample preparation bond breakage and subsequent alkylation might occur (this was also partially observed with the verified disulfide bridges). Additionally, the sequence alignment of the four IgG-like domains suggests the existence of one disulfide bridge per

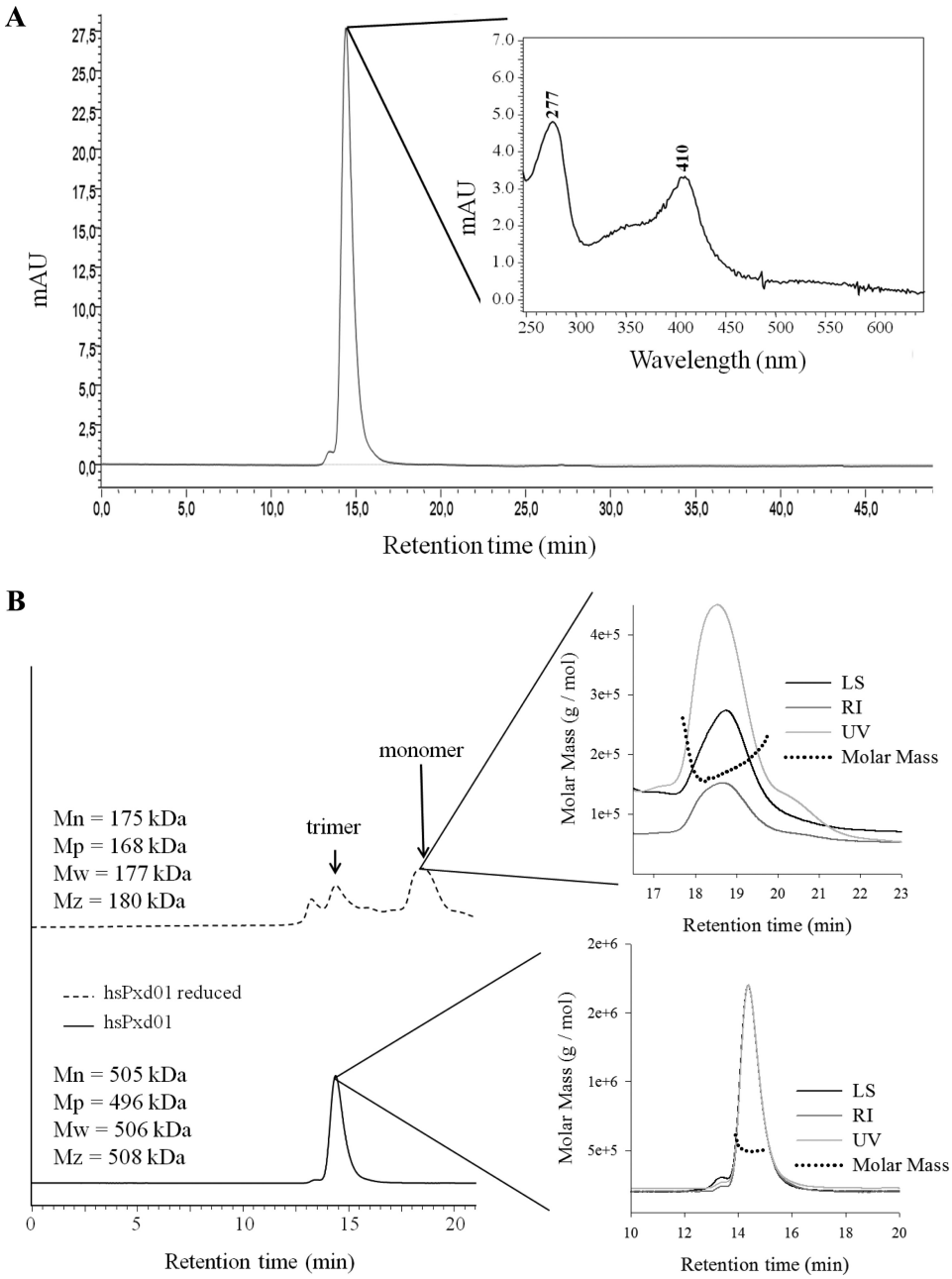

FIGURE 3. **Oligomeric structure of human peroxidasin 1.** *A,* SEC of recombinant hsPxd01. The *inset* depicts the UV-visible spectrum of the fraction eluting at 14.5 min. *B,* comparison of SECs of hsPxd01 obtained under nonreducing and reducing conditions (*dotted line*). Representative peak analyses using MALS (software ASTRA) are shown, including the calculated molar masses of the trimeric and monomeric states of hsPxd01. *mAU*, milliabsorbance units.

β-barrel structure. Regarding the proposed cystines in the VWC domain it has to be mentioned that its sequence recovery was poor, which might explain that the respective peptides were not found. In general, due to the complex sequence of hsPxd01, attaining a good sequence mapping is quite challenging because the obtained peptides were either rather big or very small. This was the reason for using both pepsin and trypsin in a sequential manner.

Heme Cavity Architecture—To gain further insight into the heme cavity architecture of hsPxd01, we probed its redox properties by spectroelectrochemistry. This allowed the comparison of peroxidasin 1 with other mammalian peroxidases (MPO, LPO, and EPO) and a prediction of the catalytic ability of the enzyme especially regarding the oxidation of halides ($Cl^- < Br^- < I^-$). Fig. 6*A* shows the spectral transition upon electrochemical reduction of ferric to ferrous hsPxd01 at pH 7.4 and 25 °C. There was a clear direct transition to ferrous hsPxd01 with a Soret maximum at 420 nm and additional bands at 523 and 553 nm and isosbestic points at 413 and 510 nm. The slope of the corresponding Nernst plot (Fig. 6*B*) is close to the theoretical value for a redox equilibrium involving the exchange of a single electron. The reduction potential of the Fe(III)/Fe(II) couple at pH 7.4 and 25 °C was calculated to be -233 ± 5 mV, which is more negative than that reported for bovine LPO

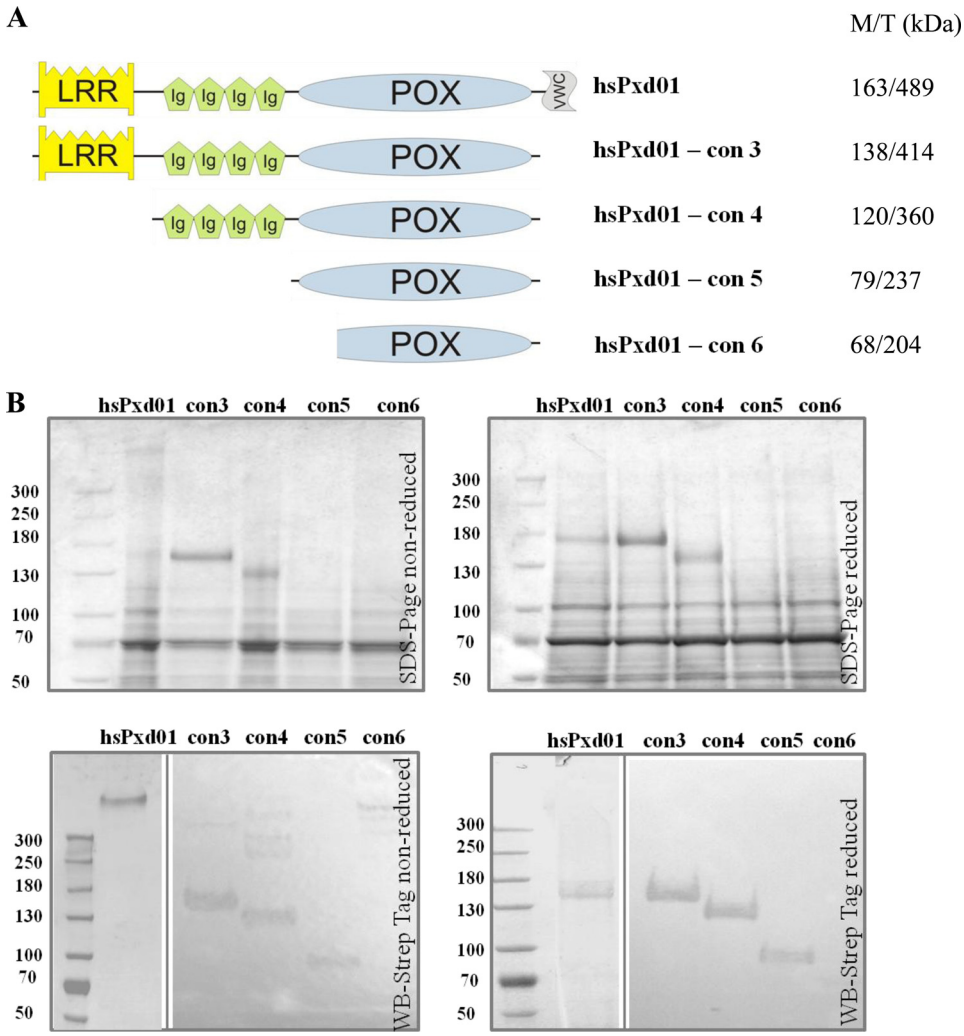

FIGURE 4. **SDS-PAGE of human peroxidasin 1 and four (truncated) constructs under nonreducing and reducing conditions.** *A, hsPxd01* is full-length protein; *hsPxd01-con3* lacks the VWC domain; *hsPxd01-con4* lacks LRR and VWC domains; *hsPxd01-con5* represents the peroxidase domain only including the "propeptide region"; *hsPxd01-con6* represents the peroxidase domain without the "propeptide region." Additionally, the molar masses of the respective (unglycosylated) proteins in the monomeric and (putative) trimeric states are presented. *B,* electrophoresis of recombinant proteins produced in HEK 293E cells under denaturating and either nonreducing (*left panels*) or reducing (*right panels*) conditions. Gels were stained with Coomassie Blue (*upper panels*) as well as immunoblotted and detected with anti-Strep antibody (*lower panels*).

(*i.e.* −176 to −190 mV) (28, 34) or human MPO (5 mV) (27). In case of the construct hsPxd01-con4, the corresponding E'_0 value was determined to be −215 ± 10 mV.

Thermal Stability and Bromination Activity of Human Peroxidasin 1—Both ECD and DSC were used to probe the thermal stability of the full-length protein as well as hsPxd01-con4 (Fig. 7). These complementary methods allow determination of the unfolding pathway of this multidomain protein. They provide crucial information about stability of and cross-talk between the individual domains of hsPxd01, which might be important for understanding the interaction with its physiological reaction partner(s).

The loss of secondary structure at 208 nm by ECD shows that significant loss of ellipticity already starts around 40 °C and ends around 70 °C suggesting a multistep noncooperative unfolding pathway (Fig. 7*A*). By contrast, the ellipticity at the heme Soret band at 412 nm (reflecting unfolding events in the heme cavity of the peroxidase domain) changed within 45 and 60 °C (estimated T_m at 52.2 °C) (Fig. 7*B*).

To get more detailed information about the unfolding pathway of hsPxd01 and hsPxd01-con4 (Ig-Ig-Ig-Ig-POX), DSC experiments were performed (Fig. 7, *C* and *D*). The thermogram of full-length hsPxd01 is complex and is best fitted by the assumption of a noncooperative (non-two-state or multiple state) transition that includes four distinct unfolding steps. Best fitting is obtained with four endotherms with T_m values of 51.5, 61.1, 69.1, and 77.5 °C, respectively. Because ellipticity in the heme region is lost between 46 and 60 °C (Fig. 7*B*), it is reasonable to assume that the peroxidase domain has the lowest thermal stability of this multidomain protein with a T_m value at ~51–52 °C.

Fig. 7*D* shows the thermogram of hsPxd01-con4 fitted with a noncooperative (non-two-state) transition of two distinct unfolding steps. The obtained T_m values are 55.5 and 67.8 °C, thereby substantiating the peroxidase domain of hsPxd01 as the domain with the lowest melting point and identifying the T_m value of the Ig domain around 68 °C.

Finally, the enzymatic activity of hsPxd01 and hsPxd01-con4 was probed (Fig. 8). The few available publications about the

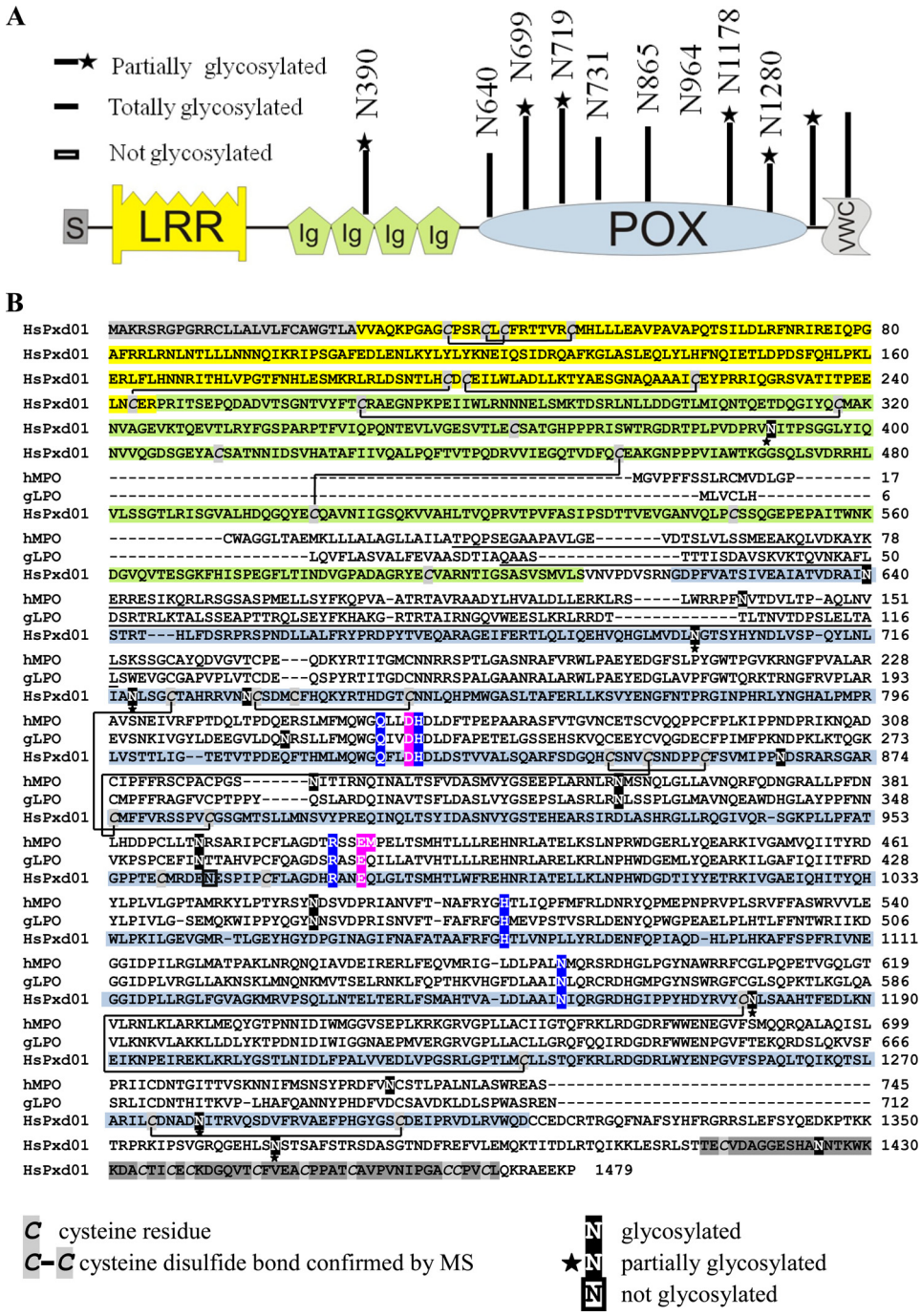

FIGURE 5. ***N*-Glycosylation and disulfide pattern of human peroxidasin 1.** *A*, schematic presentation of glycosylation sites of hsPxd01. *B*, multiple sequence alignment (Clustal X, version 1.81) of hsPxd01 with human myeloperoxidase (*hMPO*) and lactoperoxidase from goat (*gLPO*). The respective propeptides of hMPO and goat LPO are *underlined*. Important catalytic residues are highlighted in *blue*, and amino acid residues forming the covalent links with the prosthetic group are depicted in *red*. Cysteine residues are marked in *gray*, and *cysteines* involved in disulfide bonds (confirmed by MS spectrometry) are connected. Glycosylation sites are highlighted in *black*, and partially glycosylated residues of POX are shown in *black* and marked with *. One putative not glycosylated site on POX is *boxed* in *black*. Additionally, the distinct domains are marked by different coloring (signal peptide, *gray*; LRR, *yellow*; Ig, *green*; POX, *blue*; VWC, light gray). Please note that the background highlight colors for different sections of the sequence alignment match the domain coloring indicated in the *upper panel*.

halogenation activity of human peroxidasin 1 (12, 13, 15) are puzzling, because the reported activities are very low compared with chordata peroxidases, including LPO, EPO, and MPO. This observation is somehow contradictory to the high sequence similarity and the presence of all essential amino acids in the active site of subfamily 1 and 2 proteins (see also Figs. 1 and 5). Thus, to examine the kinetics of oxidation of bromide, the effect on the initial rate of bromination of NADH was measured at varying concentrations of bromide and hydrogen peroxide. This assay is very sensitive, and it allowed the detection of apparent kinetic constants of both hsPxd01 and hsPxd01-con4 (Fig. 8). Saturation kinetics behavior was observed in the presence of 5 mM bromide and varying hydrogen peroxide concentrations as well as in the presence of 50 μM hydrogen per-

TABLE 1
Relative occupancy for the 10 *N*-glycan sites of recombinant human peroxidasin 1
For comparison, also see Fig. 5.

	N- Glycosylation site(w/wo propeptide)	Peptides identified	Peptide mass (m/z)	Digest	Occupancy	Glycosylation status
1	390/364	PRV**nIT**PSGGL	556.3089	Pepsin	76% glycosylated	partially glycosylated
		PRV**NIT**PSGGL	555.8176		24% not glycosylated	
		nITPSGGLYIQnV	459.9093	Trypsin	79% glycosylated	
		PRV**NIT**PSGGLYIQnVVQGDS	753.3792		21% not glycosylated	
2	640/614	TVDRAI**n**	395.2089	Pepsin	100% glycosylated	glycosylated
		VDRAI**nST**RTHL	346.6894			
		VDRAI**nST**RTHL	461.9164			
		RAI**nST**RTHL	390.5502			
		I**nST**RTHLFD	603.8048			
		AI**nST**R	331.6784	Trypsin	100% glycosylated	
3	699/673	VDL**nGT**SY	869.3898	Pepsin	80% glycosylated	partially glycosylated
		GLmVDL**NGT**	468.2295		20% not glycosylated	
4	719/693	IA**N**	317.1821	Pepsin	100% not glycosylated	partially glycosylated
		NLIA**NL**	329.2061			
		nLIA**nLS**GCTAHRRVNnCS	720.6631	Trypsin	13% glycosylated	
		LIA**NLS**	315.6951		87% not glycosylated	
5	731/705	RVN**nCS**DMCFHQK	566.2361	Trypsin	100% glycosylated	glycosylated
		VN**nCS**DMCFHQK	514.2036			
6	865/839	NVCSNDPPCFSVMIPP**nDS**RA	565.4999	Pepsin	100% glycosylated	glycosylated
7	964/938	RDE**NES**PIPCF	682.3018	Pepsin	100% not glycosylated	not glycosylated
		ATGPPTECmRDE**NES**PIPCFLAGDHR	744.0742	Trypsin	100% not glycosylated	
		DE**NES**PIPCFLAGDHRA	619.6126			
8	1178/1152	VYC**nLS**AAHTFEDLK	590.2789	Trypsin	95.54% glycosylated	partially glycosylated
		VYC**NLS**AAHTFEDLK	589.9488		4.46% not glycosylated	
9	1280/1254	NAD**nIT**RV	452.2302	Pepsin	100% glycosylated	partially glycosylated
		NAD**nIT**RVQSD	666.824			
		ILCDNAD**nIT**RV	653.309	Trypsin	72% glycosylated	
		ILCDNAD**NIT**RV	652.8183		28% not glycosylated	
10	1368/1342	GRQGEHLS**N**	520.7517	Pepsin	100% not glycosylated	partially glycosylated
		qGEHLS**nST**SAF	631.2713	Trypsin	100% glycosylated	
		qGEHLS**nST**SAFSTR	535.9095			
		GEHLS**nST**SAF	575.7543			
11	1425/1393	LSTTECVDAGGESHA**nNT**K	664.623	Trypsin	100% glycosylated	glycosylated

oxide and different bromide concentrations. The bromination rate of NADH did not depend on NADH concentration and was entirely related to the rate of hypobromous acid production by hsPxd01 and hsPxd01-con4 as reported in the literature (30, 31). Table 3 summarizes the apparent kinetic constants K_M^{app}, k_{cat}, and k_{cat}/K_M^{app} obtained from these curves. Interestingly, the K_M^{app} values for both H_2O_2 and Br^- for hsPxd01 and hsPxd01-con4 were similar (Table 3), whereas the k_{cat} values of hsPxd01-con4 were more than 15 times higher.

DISCUSSION

The interest in human peroxidasin 1 has increased rapidly over the last years especially since the discovery of its essential role in the formation of collagen IV cross-links (13, 15). It has

TABLE 2

Oxidation status of cysteines of recombinant human peroxidasin 1

The corresponding peptide sequences and MS details are given.

Cysteine status	Peptide sequences and locations	*m/z*	Error	Peak height (counts)
			ppm	
Alkylated cysteine (Cys^{12})	^{7}GPGRRCL^{13}	815.4291	−1.7	99,640
Alkylated cysteine (Cys^{20})	^{17}VLFCAW^{22}	795.3889	4.3	10,731
Disulfide bond (Cys^{36}–Cys^{42})	^{26}AVVAQKPGAGCPSR^{39} + ^{40}CLCF^{43} + ^{49}CMHL^{52}	581.5230	1.7	61,830
Disulfide bond (Cys^{40}–Cys^{49})				
Disulfide bond (Cys^{40}–Cys^{49})	^{40}CL^{41} + ^{45}TTVRCMHL^{52}	1192.5695	4.6	496,491
Disulfide bond (Cys^{196}–Cys^{243})	^{195}HCDCEILW^{202} + ^{242}NCERPR^{247} + ^{222}CEYPRRIQGR^{231}	1532.6970	−0.1	4715
Disulfide bond (Cys^{198}–Cys^{222})				
Disulfide bond (Cys^{267}–Cys^{317})	^{265}FTCR^{268} + ^{315}YQCMAKNVAGEVK^{327}	982.4679	4.5	4531
Disulfide bond (Cys^{454}–Cys^{502})	^{453}QCEAK^{457} + ^{495}HDQGQYECQAVNII^{508}	549.0033	9.9	260,843
Alkylated cysteine (Cys^{502})	^{501}ECQAVNIIGSQK^{512}	673.8504	7.2	833,089
Disulfide bond (Cys^{723}–Cys^{885})	^{718}ANLSGCTAHRRVNNCSDMCF^{737} + ^{881}SSPVCGSGMTSLLMNSVYPREQI^{903} + ^{741}YRTHDGTCNNL^{751}	1189.7363	5.8	4632
Disulfide bond (Cys^{732}–Cys^{748})				
Alkylated cysteine (Cys^{736})	^{729}VNNCSDMCF^{737}	545.1964	4.9	49,406
Disulfide bond (Cys^{732}–Cys^{748})	^{729}VNNCSDMCF^{737} + ^{743}THDGTCNNLQHPMWGASL^{760}	1506.0912	−9.6	4455
Disulfide bond (Cys^{847}–Cys^{857})	^{842}SDGQHCSNVCSNDPPCF^{858} + ^{875}CMF^{877}	1102.8999	13.9	24,306
Disulfide bond (Cys^{851}–Cys^{875})				
Alkylated cysteine (Cys^{970})	^{962}DENESPIPCF^{971}	403.1687	−1.7	9367
Disulfide bond (Cys^{1177}–Cys^{1234})	^{1177}CNLSAAHTF^{1185} + ^{1229}GPTLMCL^{1235}	847.8858	−3.4	5330
Alkylated cysteine (Cys^{1234})	^{1229}GPTLMCL^{1235}	791.3769	−2.7	5841
Disulfide bond (Cys^{1275}–Cys^{1301})	^{1273}ILCDNADNI^{1281} + ^{1299}GSCDEIPRVDLR^{1310}	1174.0454	−9.6	4376
Alkylated cysteine (Cys^{1275})	^{1273}ILCDNADNI^{1281}	524.2406	−3.9	72,256
3 Alkylated cysteines (Cys^{1315}, Cys^{1316}, Cys^{1319})	^{1310}RVWQDCCEDCR^{1320}	528.5469	6.0	2449
Alkylated cysteine (Cys^{1415})	^{1410}LSTTECVDAGGESHANNTKWK^{1430}	577.0208	3.9	65,856

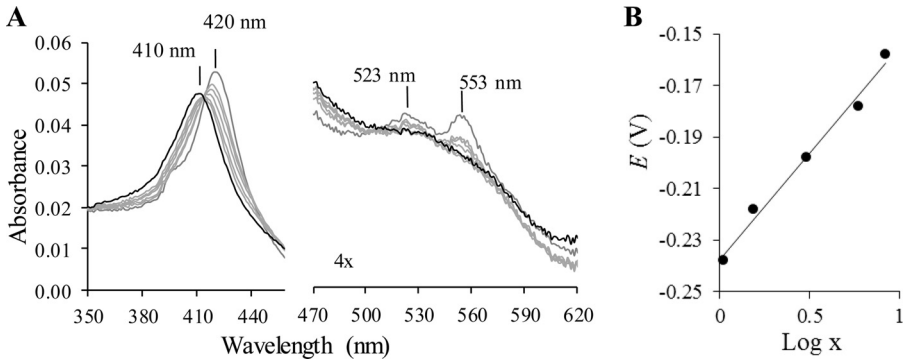

FIGURE 6. **Spectroelectrochemistry of human peroxidasin 1.** *A,* electronic spectra of hsPxd01 obtained at various potentials in spectroelectrochemical experiments (100 mM phosphate buffer, pH 7.4, including 100 mM NaCl). *B,* corresponding Nernst plot is reported, where *X* represents $((A_{\lambda red}{}^{max} - A_{\lambda red})/(A_{\lambda ox}{}^{max} - A_{\lambda ox}))$ with λ_{ox} = 410 nm and λ_{red} = 420 nm, respectively.

been shown that the absence of the enzyme has severe and fatal impacts in model organisms (5, 6, 15), but detrimental mutations in humans have also been reported (35, 36). Therefore, a better understanding of the biochemical function and biophysical properties can be of crucial importance.

Sequence analysis of the multidomain subunit structure of hsPxd01 suggested the occurrence of one enzymatic domain with homology to mammalian peroxidases (3). Similar to the latter, the heme in hsPxd01 is post-translationally modified and covalently linked to acidic amino acids (Asp-826 and Glu-980) (3, 37). The proximal heme ligand histidine is likely hydrogen-bonded to an asparagine, and at the distal heme cavity all catalytic residues (His-827, Gln-823, and Arg-977) are found (3). The His/Arg pair is involved in the heterolytic cleavage of hydrogen peroxide during compound I formation, whereas the glutamine residue is involved in the binding of halides (3). As a consequence, the observed spectral (Soret band at 410 nm, high spin ferric state) and redox properties of hsPxd01 are comparable with LPO. The reduction potential of the Fe(III)/Fe(II) couple of −233 ± 5 mV is more negative compared with LPO (*i.e.* −176 to −190 mM) (28, 34), EPO (−126 mV) (28), or MPO (5 mV) (27).

N-Glycosylation occupancy of the peroxidase domain of hsPxd01 could be verified at seven positions. This matches with five *N*-glycans in mature homodimeric MPO and pro-MPO produced in CHO cell lines (21). Monomeric bovine lactoperoxidase has four *N*-glycosylation sites (38). Furthermore, the peroxidase domain of hsPxd01 was shown to be stabilized by seven confirmed disulfide bridges, including the propeptide region. One predicted disulfide bond in the peroxidase domain (Cys-959–Cys-970) could not be confirmed; however, there was also no free Cys-959 detected. In hsPxd01, this region is part of the polypeptide chain, whereas in mammalian peroxidases (which have no additional domains), it is proteolytically cleaved off during maturation. In MPO there are six intra-chain disulfide bridges (and one between the two subunits), whereas monomeric LPO is stabilized by seven cystines. Together with the recently published phylogenetic studies (39), these findings

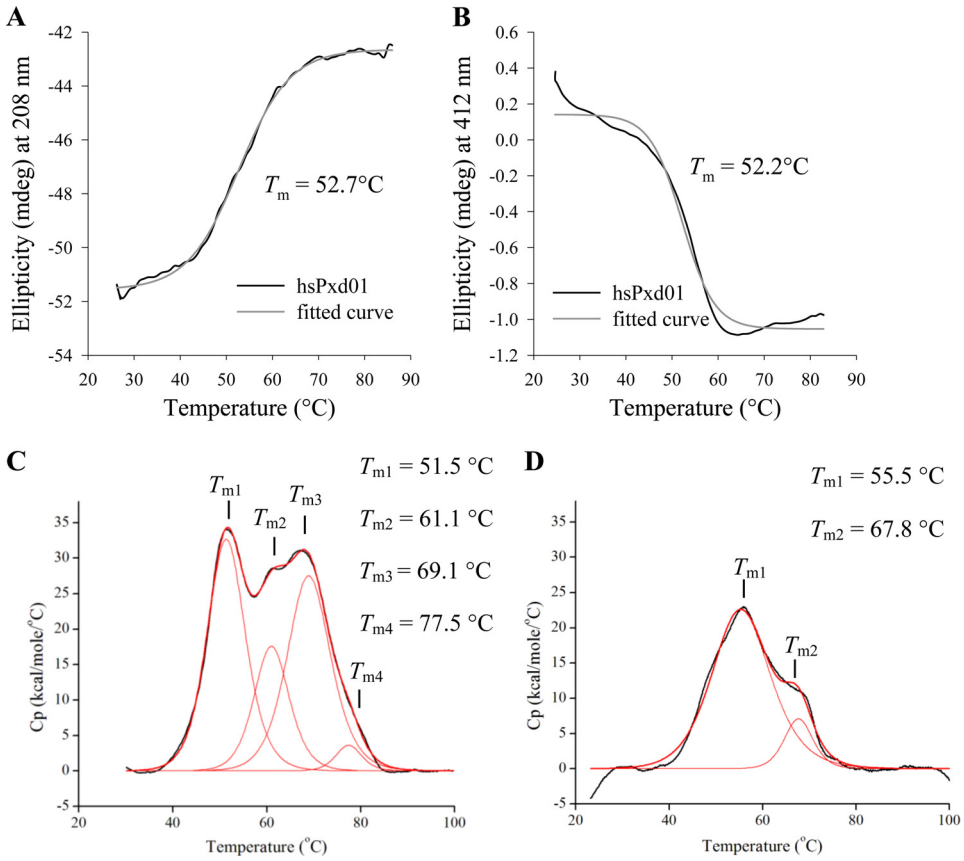

FIGURE 7. **Thermal stability of human peroxidasin 1.** *A,* temperature-mediated unfolding of hsPxd01 followed by ECD spectroscopy at 208 nm. The corresponding fit is depicted in *gray*. *B,* temperature-mediated unfolding of hsPxd01 followed by ECD spectroscopy at 412 nm. The corresponding fit is depicted in *gray*. Temperature-mediated unfolding of hsPxd01 (*C*) and hsPxd01-con4 (*D*) followed by differential scanning calorimetry. Original DSC data are depicted in *black*. Fitting of data (*red lines*) suggests the occurrence of four consecutive unfolding events. The corresponding midterm transition temperatures (T_m values) are depicted.

suggest a similar overall (mainly α-helical) structure as well as heme cavity architecture of the peroxidase domain of hsPxd01 (Fig. 5).

Besides the heavily glycosylated peroxidase domain, three additional glycosylation positions could be verified at the second immunoglobulin domain, the linker between the peroxidase and VWC domain as well as at the von Willebrand factor C domain. Four intradomain cystines could be identified by MS analysis in the LRR region and two in the Ig domains.

Furthermore, we could demonstrate that hsPxd01 is a homotrimeric oxidoreductase. This corresponds to the overall structure of peroxidasin from *D. melanogaster* reported by Nelson *et al.* in 1994 (4). Analyses of molar masses of the full-length protein (504 kDa) and truncated versions under oxidized and reduced conditions clearly demonstrated that hsPxd01 is a homotrimeric protein having the protomers covalently bound via (redox-sensitive) cystine bridges at their C-terminal VWC domains. One might speculate whether this trimeric structure of hsPxd01 is related to the fact that type IV collagen before post-translational modification is also a (hetero)trimeric protein. Peroxidasin 1 has been reported to cross-link these triple-helical protomers into oligomers. In detail, during this process hsPxd01 should be responsible for cross-linking two opposing C-terminal NC1 trimers of collagen IV to form a hexameric dimer (13). This collagen "knot" (covalent sulfilimine bonds between Met-93 and Lys-211 at the interface of adjoining protomers) is synthesized by hsPxd01 by the release of hypobromous acid (15). To allow such a specific reaction, a close interaction between the three-armed hsPxd01 and the C termini of the collagen IV protomers must occur. Furthermore, a close proximity between the enzyme and NC1 protomers reduces the oxidative damage by hindering accidental scavenging of hypobromous acid by other residues. One might speculate whether the additional domains (LRR and Ig domains) mediate a suitable distance and orientation by protein-protein interactions.

Compared with myeloperoxidase (40) and lactoperoxidase (41), human peroxidasin 1 shows several intermediate states during temperature-mediated unfolding. This reflects the multidomain architecture of this peculiar peroxidase but also suggests a noncooperative unfolding pathway that might indicate loose interaction between the individual domains. This flexibility could support the interaction of hsPxd01 with the protomers of trimeric collagen IV as described above.

Based on the homology with the human peroxidases and the fact that those efficiently mediate the two-electron oxidation of halides, it was speculated that hsPxd01 also catalyzes the formation of hypohalous acids. The available data from the literature are puzzling and mostly based on end-point determinations after long incubation of hsPxd01 with halides and

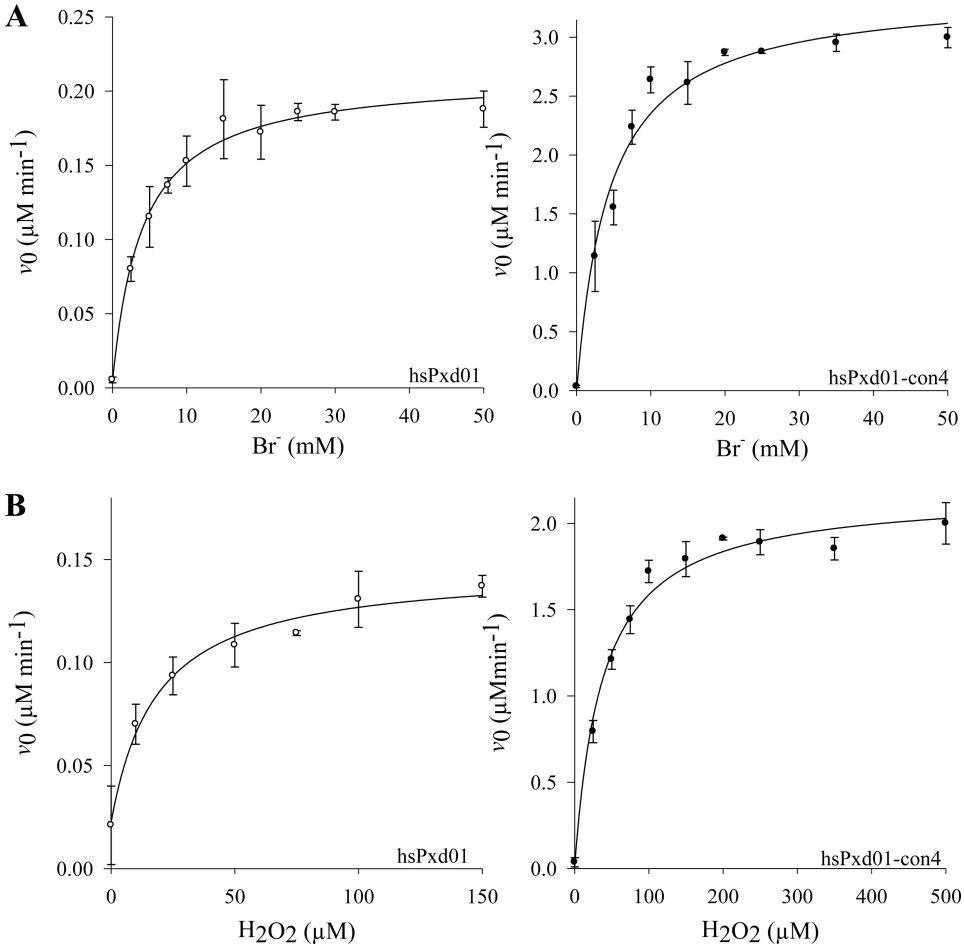

FIGURE 8. **Rate of NADH bromohydrin formation by human peroxidasin 1.** 100 nM enzyme full-length hsPxd01 (○) or the construct hsPxd01-con4 (●) were incubated at 25 °C in 20 mM phosphate buffer, pH 7.4, containing 100 μM NADH with either 50 μM H_2O_2 with varying concentrations of NaBr (*A*) or 5 mM NaBr with varying concentrations of H_2O_2 (*B*). The formation of bromohydrin was detected by absorbance at 275 nm, and initial rates were determined within the first 1 min. Data show means of triplicates.

TABLE 3

Kinetic parameters for the formation of NADH bromohydrin by recombinant human peroxidasin 1 (hsPxd01) and the construct hsPxd01-con4 in 100 mM phosphate buffer, pH 7.4, and 25 °C

hsPxd01		hsPxd01-con4	
H_2O_2			
K_M^{app}	18.6 ± 4.6 μM	K_M^{app}	37.7 ± 6.0 μM
V_{max}^{app}	0.12 ± 0.01 μM min^{-1}	V_{max}^{app}	2.2 ± 0.5 μM min^{-1}
k_{cat}	1.2 min^{-1}	k_{cat}	22 min^{-1}
k_{cat}/K_M^{app}	6.5 × 10^4 $M^{-1}min^{-1}$	k_{cat}/K_M^{app}	5.8 × 10^5 $M^{-1}min^{-1}$
Br^-			
K_M^{app}	4.1 ± 0.5 mM	K_M^{app}	4.4 ± 0.8 mM
V_{max}^{app}	0.21 ± 0.01 μM min^{-1}	V_{max}^{app}	3.4 ± 0.2 μM min^{-1}
k_{cat}	2.1 min^{-1}	k_{cat}	34 min^{-1}
k_{cat}/K_M^{app}	5.1 × 10^2 $M^{-1}min^{-1}$	k_{cat}/K_M^{app}	7.7 × 10^3 $M^{-1}min^{-1}$

hydrogen peroxide (12, 13, 15). In this study, for the first time the steady-state kinetics of bromide oxidation at physiological pH 7.4 was examined. Oxidation of chloride (140 mM) at pH 7.4 was negligible (data not shown), which is closely related to the hierarchy of the reduction potential of the Fe(III)/Fe(II) couple (*i.e.* hsPxd01 < LPO < EPO ≪ MPO) and the fact that hsPxd01 as well as LPO or EPO are not able to form the electron-withdrawing sulfonium ion heme to protein linkage. The latter is typical for MPO and its strong oxidation capacity (42–44). However, bromide oxidation by hsPxd01 and hsPxd01-con4 could be monitored continuously and shown to depend on both the hydrogen peroxide as well as the bromide concentration (Fig. 8). This (for the first time) allowed us to determine apparent enzymatic parameters. Interestingly, the K_M^{app} values for bromide were similar for both hsPxd01 (4.1 mM) and hsPxd01-con4 (4.4 mM), which reflects the similar spectral and redox properties (and thus heme cavity architecture) for both proteins. Nevertheless, compared with mammalian peroxidases, the apparent catalytic efficiency of bromide oxidation by hsPxd01 is relatively low. Based on the same assay, the apparent catalytic efficiency of bromide oxidation of hsPxd01-con4 is only about 1% compared with MPO (32). But most interestingly

(despite the fact that it binds bromide with the same affinity), the full-length enzyme is even less active. This discrepancy is surprising at first sight but could be related to the physiological role of hsPxd01 described above. In contrast to the human peroxidases, which are involved in the innate immune system and release antimicrobial hypohalous acids at high flux, such an uncontrolled reactivity would be deleterious for a biosynthetic oxidation of distinct (hydroxyl)lysine and methionine residues.

Because there is no x-ray structure of neither full-length hsPxd01 nor a truncated version so far available, one can only speculate about necessary conformational changes that occur upon binding of hsPxd01 to collagen IV thereby increasing the accessibility of the heme cavity. Most probably the structural differences between monomeric hsPxd01-con4 and trimeric full-length hsPxd01 are related to substrate accessibility rather than differences in the heme cavity.

Clearly more studies are necessary to probe this hypothesis. Together with TPO (45), peroxidasins represent peroxidases that are not primarily related with defense of the mature organism (like LPO, EPO, and MPO that release freely diffusing hypohalous acids) but with biosynthetic tasks. In both cases, the target proteins (thyroglobulin and collagen IV) are not able to enter the active site but will be modified specifically by mobile oxidants (hypoiodous acid and hypobromous acid). Understanding theses reactions at a molecular level will be a great challenge in the future.

Acknowledgments—We thank Professor J.-C. Michalsky and M.-C. Slomianny from Unité Mixte de Recherche CNRS/USTL 8576, Glycobiologie Structurale et Fonctionnelle, Université des Sciences et Technologies de Lille 1, Villeneuve d'Ascq, France for their help.

REFERENCES

1. Davies, M. J., Hawkins, C. L., Pattison, D. I., and Rees, M. D. (2008) Mammalian heme peroxidases: from molecular mechanisms to health implications. *Antioxid. Redox Signal.* **10,** 1199–1234
2. Ruf, J., and Carayon, P. (2006) Structural and functional aspects of thyroid peroxidase. *Arch. Biochem. Biophys.* **445,** 269–277
3. Zamocky, M., Jakopitsch, C., Furtmüller, P. G., Dunand, C., and Obinger, C. (2008) The peroxidase-cyclooxygenase superfamily: reconstructed evolution of critical enzymes of the innate immune system. *Proteins* **72,** 589–605
4. Nelson, R. E., Fessler, L. I., Takagi, Y., Blumberg, B., Keene, D. R., Olson, P. F., Parker, C. G., and Fessler, J. H. (1994) Peroxidasin: a novel enzyme-matrix protein of *Drosophila* development. *EMBO J.* **13,** 3438–3447
5. Gotenstein, J. R., Swale, R. E., Fukuda, T., Wu, Z., Giurumescu, C. A., Goncharov, A., Jin, Y., and Chisholm, A. D. (2010) The *C. elegans* peroxidasin PXN-2 is essential for embryonic morphogenesis and inhibits adult axon regeneration. *Development.* **137,** 3603–3613
6. Tindall, A. J., Pownall, M. E., Morris, I. D., and Isaacs, H. V. (2005) *Xenopus tropicalis* peroxidasin gene is expressed within the developing neural tube and pronephric kidney. *Dev. Dyn.* **232,** 377–384
7. Cheng, G., Salerno, J. C., Cao, Z., Pagano, P. J., and Lambeth, J. D. (2008) Identification and characterization of VPO1, a new animal heme-containing peroxidase. *Free Radic. Biol. Med.* **45,** 1682–1694
8. Péterfi, Z., Donkó, A., Orient, A., Sum, A., Prókai, A., Molnár, B., Veréb, Z., Rajnavölgyi E., Kovács, K. J., Müller, V., Szabó, A. J., and Geiszt, M. (2009) Peroxidasin is secreted and incorporated into the extracellular matrix of myofibroblasts and fibrotic kidney. *Am. J. Pathol.* **175,** 725–735
9. Péterfi, Z., Tóth, Z. E., Kovács, H. A., Lázár, E., Sum, A., Donkó, A., Sirokmány, G., Shah, A. M., and Geiszt, M. (2014) Peroxidasin-like protein: a novel peroxidase homologue in the human heart. *Cardiovasc. Res.* **101,** 393–399
10. Liu, Y., Carson-Walter, E. B., Cooper, A., Winans, B. N., Johnson, M. D., and Walter, K. A. (2010) Vascular gene expression patterns are conserved in primary and metastatic brain tumors. *J. Neurooncol.* **99,** 13–24
11. Cheng, G., Li, H., Cao, Z., Qiu, X., McCormick, S., Thannickal, V. J., and Nauseef, W. M. (2011) Vascular peroxidase-1 is rapidly secreted, circulates in plasma, and supports dityrosine cross-linking reactions. *Free Radic. Biol. Med.* **51,** 1445–1453
12. Li, H., Cao, Z., Zhang, G., Thannickal, V. J., and Cheng, G. (2012) Vascular peroxidase 1 catalyzes the formation of hypohalous acids: characterization of its substrate specificity and enzymatic properties. *Free Radic. Biol. Med.* **53,** 1954–1959
13. Bhave, G., Cummings, C. F., Vanacore, R. M., Kumagai-Cresse, C., Ero-Tolliver, I. A., Rafi, M., Kang, J.-S., Pedchenko, V., Fessler, L. I., Fessler, J. H., and Hudson, B. G. (2012) Peroxidasin forms sulfilimine chemical bonds using hypohalous acids in tissue genesis. *Nat. Chem. Biol.* **8,** 784–790
14. Fidler, A. L., Vanacore, R. M., Chetyrkin, S. V., Pedchenko, V. K., Bhave, G., Yin, V. P., Stothers, C. L., Rose, K. L., McDonald, W. H., Clark, T. A., Borza, D.-B., Steele, R. E., Ivy, M. T., Aspirnauts, Hudson, J. K., and Hudson, B. G. (2014) A unique covalent bond in basement membrane is a primordial innovation for tissue evolution. *Proc. Natl. Acad. Sci. U.S.A.* **111,** 331–336
15. McCall, A. S., Cummings, C. F., Bhave, G., Vanacore, R., Page-McCaw, A., and Hudson, B. G. (2014) Bromine is an essential trace element for assembly of collagen IV scaffolds in tissue development and architecture. *Cell* **157,** 1380–1392
16. Lambert, C., Léonard, N., De Bolle, X., and Depiereux, E. (2002) ESyPred3D: Prediction of proteins 3D structures. *Bioinformatics* **18,** 1250–1256
17. Graham, F. L., and van der Eb, A. J. (1973) A new technique for the assay of infectivity of human adenovirus 5 DNA. *Virology* **52,** 456–467
18. Tom, R., Bisson, L., and Durocher, Y. (2008) Culture of HEK293-EBNA1 cells for production of recombinant proteins. *CSH Protoc.* 10.1101/pdb.prot4976
19. Tom, R., Bisson, L., and Durocher, Y. (2008) Transfection of HEK293-EBNA1 cells in suspension with linear PEI for production of recombinant proteins. *CSH Protoc.* 10.1101/pdb.prot4979
20. Feissner, R., Xiang, Y., and Kranz, R. G. (2003) Chemiluminescent-based methods to detect subpicomole levels of c-type cytochromes. *Anal. Biochem.* **315,** 90–94
21. Van Antwerpen, P., Slomianny, M.-C., Boudjeltia, K. Z., Delporte, C., Faid, V., Calay, D., Rousseau, A., Moguilevsky, N., Raes, M., Vanhamme, L., Furtmüller, P. G., Obinger, C., Vanhaeverbeek, M., Nève, J., and Michalski, J.-C. (2010) Glycosylation pattern of mature dimeric leukocyte and recombinant monomeric myeloperoxidase: glycosylation is required for optimal enzymatic activity. *J. Biol. Chem.* **285,** 16351–16359
22. Jensen, L. J., Gupta, R., Blom, N., Devos, D., Tamames, J., Kesmir, C., Nielsen, H., Staerfeldt, H. H., Rapacki, K., Workman, C., Andersen, C. A., Knudsen, S., Krogh, A., Valencia, A., and Brunak, S. (2002) Prediction of *N*-glycosylation sites in human proteins. *J. Mol. Biol.* **319,** 1257–1265
23. Delporte, C., Boudjeltia, K. Z., Noyon, C., Furtmüller, P. G., Nuyens, V., Slomianny, M.-C., Madhoun, P., Desmet, J.-M., Raynal, P., Dufour, D., Koyani, C. N., Reyé, F., Rousseau, A., Vanhaeverbeek, M., Ducobu, J., *et al.* (2014) Impact of myeloperoxidase-LDL interactions on enzyme activity and subsequent posttranslational oxidative modifications of apoB-100. *J. Lipid Res.* **55,** 747–757
24. Stoll, S., and Schweiger, A. (2006) EasySpin, a comprehensive software package for spectral simulation and analysis in EPR. *J. Magn. Reson.* **178,** 42–55
25. Peisach, J., Blumberg, W. E., Ogawa, S., Rachmilewitz, E. A., and Oltzik, R. (1971) The effects of protein conformation on the heme symmetry in high spin ferric heme proteins as studied by electron paramagnetic resonance. *J. Biol. Chem.* **246,** 3342–3355
26. Battistuzzi, G., Borsari, M., Ranieri, A., and Sola, M. (2002) Redox thermodynamics of the Fe^{3+}/Fe^{2+} couple in horseradish peroxidase and its cyanide complex. *J. Am. Chem. Soc.* **124,** 26–27
27. Battistuzzi, G., Bellei, M., Zederbauer, M., Furtmüller, P. G., Sola, M., and

Obinger, C. (2006) Redox thermodynamics of the Fe(III)/Fe(II) couple of human myeloperoxidase in its high spin and low-spin forms. *Biochemistry* **45,** 12750–12755
28. Battistuzzi, G., Bellei, M., Vlasits, J., Banerjee, S., Furtmüller, P. G., Sola, M., and Obinger, C. (2010) Redox thermodynamics of lactoperoxidase and eosinophil peroxidase. *Arch. Biochem. Biophys.* **494,** 72–77
29. Auer, M., Gruber, C., Bellei, M., Pirker, K. F., Zamocky, M., Kroiss, D., Teufer, S. A., Hofbauer, S., Soudi, M., Battistuzzi, G., Furtmüller, P. G., and Obinger, C. (2013) A stable bacterial peroxidase with novel halogenating activity and an autocatalytically linked heme prosthetic group. *J. Biol. Chem.* **288,** 27181–27199
30. Auchère, F., and Capeillère-Blandin, C. (1999) NADPH as a cosubstrate for studies of the chlorinating activity of myeloperoxidase. *Biochem. J.* **343,** 603–613
31. Prütz, W. A., Kissner, R., Koppenol, W. H., and Rüegger, H. (2000) On the irreversible destruction of reduced nicotinamide nucleotides by hypohalous acids. *Arch. Biochem. Biophys.* **380,** 181–191
32. Forbes, L. V., Sjögren, T., Auchère, F., Jenkins, D. W., Thong, B., Laughton, D., Hemsley, P., Pairaudeau, G., Turner, R., Eriksson, H., Unitt, J. F., and Kettle, A. J. (2013) Potent reversible inhibition of myeloperoxidase by aromatic hydroxamates. *J. Biol. Chem.* **288,** 36636–36647
33. UniProt Consortium (2015) UniProt: a hub for protein information. *Nucleic Acids Res.* **43,** D204–D212
34. Ohlsson, P. I., and Paul, K. G. (1983) The reduction potential of lactoperoxidase. *Acta Chem. Scand. B* **37,** 917–921
35. Khan, K., Rudkin, A., Parry, D. A., Burdon, K. P., McKibbin, M., Logan, C. V., Abdelhamed, Z. I., Muecke, J. S., Fernandez-Fuentes, N., Laurie, K. J., Shires, M., Fogarty, R., Carr, I. M., Poulter, J. A., Morgan, J. E., *et al.* (2011) Homozygous mutations in PXDN cause congenital cataract, corneal opacity, and developmental glaucoma. *Am. J. Hum. Genet.* **89,** 464–473
36. Choi, A., Lao, R., Ling-Fung Tang, P., Wan, E., Mayer, W., Bardakjian, T., Shaw, G. M., Kwok, P. Y., Schneider, A., and Slavotinek, A. (2015) Novel mutations in PXDN cause microphthalmia and anterior segment dysgenesis. *Eur. J. Hum. Genet.* **23,** 337–341
37. Zederbauer, M., Furtmüller, P. G., Brogioni, S., Jakopitsch, C., Smulevich, G., and Obinger, C. (2007) Heme to protein linkages in mammalian peroxidases: Impact on spectroscopic, redox and catalytic properties. *Nat. Prod. Rep.* **24,** 571–584
38. Singh, A. K., Singh, N., Sharma, S., Singh, S. B., Kaur, P., Bhushan, A., Srinivasan, A., and Singh, T. P. (2008) Crystal structure of lactoperoxidase at 2.4 Å resolution. *J. Mol. Biol.* **376,** 1060–1075
39. Soudi, M., Zamocky, M., Jakopitsch, C., Furtmüller, P. G., and Obinger, C. (2012) Molecular evolution, structure and function of peroxidasins. *Chem. Biodivers.* **9,** 1776–1793
40. Banerjee, S., Stampler, J., Furtmüller, P. G., and Obinger, C. (2011) Conformational and thermal stability of mature dimeric human myeloperoxidase and a monomeric recombinant form from CHO cells. *Biochim. Biophys. Acta* **1814,** 375–387
41. Banerjee, S., Furtmüller, P. G., and Obinger, C. (2011) Lactoperoxidase–a versatile one- and two-electron catalyst of high structural and thermal stability. *Biotechnol. J.* **6,** 231–243
42. Arnhold, J., Furtmüller, P. G., and Obinger, C. (2003) Redox properties of myeloperoxidase. *Redox Rep.* **8,** 179–186
43. Arnhold, J., Monzani, E., Furtmüller, P. G., Zederbauer, M., Casella, L., and Obinger, C. (2006) Kinetics and thermodynamics of halide and nitrite oxidation by heme peroxidases. *Eur. J. Inorg. Chem.* **19,** 3801–3811
44. Battistuzzi, G., Stampler, J., Bellei, M., Vlasits, J., Soudi, M., Furtmüller, P. G., and Obinger, C. (2011) Influence of the covalent heme to protein bonds on the redox thermodynamics of human myeloperoxidase. *Biochemistry* **50,** 7987–7994
45. Kessler, J., Obinger, C., and Eales, G. (2008) Factors influencing the study of peroxidase-generated iodine species and implications for thyroglobulin synthesis. *Thyroid* **18,** 769–774

Enzymology:

Multidomain Human Peroxidasin 1 Is a Highly Glycosylated and Stable Homotrimeric High Spin Ferric Peroxidase

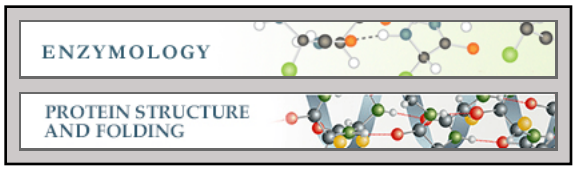

Monika Soudi, Martina Paumann-Page, Cedric Delporte, Katharina F. Pirker, Marzia Bellei, Eva Edenhofer, Gerhard Stadlmayr, Gianantonio Battistuzzi, Karim Zouaoui Boudjeltia, Paul G. Furtmüller, Pierre Van Antwerpen and Christian Obinger

J. Biol. Chem. 2015, 290:10876-10890.
doi: 10.1074/jbc.M114.632273 originally published online February 24, 2015
